IEEE Photonics Journal
An IEEE Photonics Society Publication

Numerical Analysis of Second Harmonic Generation in Soft Glass Equiangular Spiral Photonic Crystal Fibers

Volume 4, Number 2, April 2012

I. N. M. Wijeratne
N. Kejalakshmy, Member, IEEE
A. Agrawal, Member, IEEE
B. M. A. Rahman, Senior Member, IEEE
K. T. V. Grattan

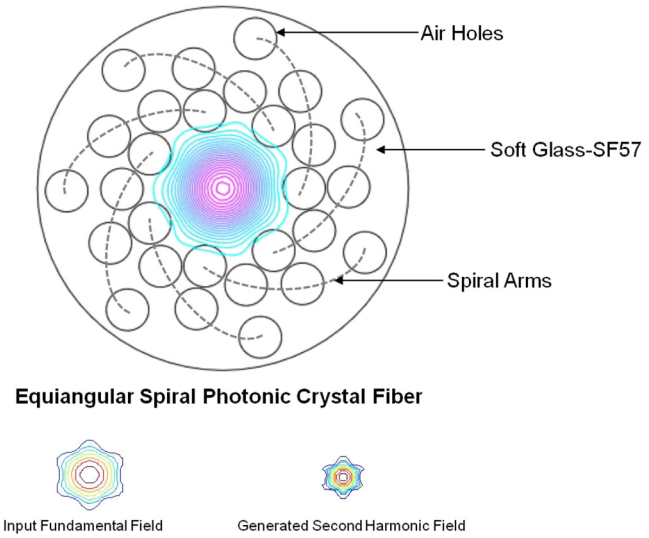

DOI: 10.1109/JPHOT.2012.2186795
1943-0655/$31.00 ©2012 IEEE

Numerical Analysis of Second Harmonic Generation in Soft Glass Equiangular Spiral Photonic Crystal Fibers

I. N. M. Wijeratne, N. Kejalakshmy, *Member, IEEE*, A. Agrawal, *Member, IEEE*, B. M. A. Rahman, *Senior Member, IEEE*, and K. T. V. Grattan

School of Engineering and Mathematical Sciences, City University London, EC1V 0HB London, U.K.

DOI: 10.1109/JPHOT.2012.2186795
1943-0655/$31.00 ©2012 IEEE

Manuscript received January 18, 2012; accepted January 27, 2012. Date of publication February 3, 2012; date of current version March 7, 2012. Corresponding author: I. N. M. Wijeratne (e-mail: bp767@city.ac.uk).

Abstract: In this paper, the accurate and numerically efficient finite element (FE)-based beam propagation method (BPM) has been employed to investigate second harmonic generation (SHG) in highly nonlinear soft glass (SF57) equiangular spiral photonic crystal fibers (ES-PCFs) for the first time. It is shown here that the SHG output power in highly nonlinear SF57 soft glass PCF exploiting the ES design is significantly higher compared with that of silica PCF with hexagonal air-hole arrangements. The effects of fabrication tolerances on the coherence length and the modal properties of ES-PCF are also illustrated. Moreover, phase matching between the fundamental and the second harmonic modes is discussed through the use of the quasi-phase matching technique. Furthermore, the ultralow bending loss in the SF57 ES-PCF design has been successfully analyzed.

Index Terms: Second harmonic generation (SHG), photonic crystal fibers (PCFs), finite element method (FEM).

1. Introduction

Recently, considerable interest has been shown in guided wave second harmonic generation (SHG) devices implementing compact short wavelength coherent light sources which would be useful across a range of applications such as optical data storage, xerography, spectroscopy, and telecommunication [1]. SHG is a nonlinear effect that comes into play with the use of sufficiently intense electromagnetic fields. The nonlinear response of a medium is related to the anharmonic motion of bound electrons under the influence of the applied electromagnetic field [2] and nonlinear processes such as SHG are a result of the second-order susceptibility denoted by χ^2. The requirements for efficient SHG include a medium with large second-order susceptibility and phase matching between the optical modes at the fundamental and second-order frequencies.

1.1. Choice of Structure

Photonic crystal fibers (PCFs) can improve the power conversion efficiency by enhancing the overlap integral between the fundamental and second harmonic modes, which is a result of unique air-hole orientation of the PCF structure [3]. These fibers have been responsible for a renaissance in the field of optical fiber devices since they were first reported in the late 1990s [4]. Generally, an index guided PCF consists of a solid central core surrounded by an array of microscopic air holes extending along the entire length of the fiber. The structure of a PCF allows the guidance of light in

the solid core by the mechanism of modified total internal reflection, which arises due to the lower equivalent index of the microstructured air-filled cladding region. Appropriate design of the microstructure of air holes allows significant flexibility in tailoring the modal and dispersion properties of a PCF, for example, in achieving small mode area (for high nonlinearity), and/or low and flat dispersion. The equiangular spiral PCF (ES-PCF) [5] provides several design parameters by which the modal properties as well as the dispersion can be controlled more easily. The ES-PCF provides better confinement of the fundamental mode in the core area than conventional PCF does. For a given material, ES-PCF achieves better overlap between the optical fields of the fundamental mode at the frequencies of interest (i.e., of the pump and second harmonic) than in conventional PCF. Hence, an ES-PCF is an excellent choice for nonlinear applications such as SHG, four-wave mixing (FWM), and supercontinuum generation.

1.2. Choice of Material

Traditionally, silica has been the material of choice for the fabrication of PCF due to its superior optical and material properties. However, the inversion symmetry of the silica glass implies that its second-order nonlinear susceptibility (χ^2) is zero. So far, various thermal poling techniques have been implemented to overcome this problem [6]–[9] which can bring the second-order susceptibility of silica glass to $d_{33} \sim 0.22$ pm/V [10]. Alternatively, commercially available lead silicate glass (also called soft glass) of type SF57 (manufactured by Schott) can achieve a much higher second-order susceptibility tensor value (of $d_{33} \sim 0.35$ pm/V) when the electron-beam irradiation technique is applied[1] [11], [12]. Therefore, SF57, which is the earliest available single mode non-silica glass PCF, is a promising candidate material for SHG. Further, SF57-based PCF has been reported to have the highest nonlinearity in optical fibers (640 $W^{-1}km^{-1}$) [13]. Also, challenging structures such as nanowires have been fabricated using SF57 glass [14]. This glass also possesses a higher thermal expansion coefficient (9.2×10^{-6} K^{-1} [15]) compared to that of silica ($\sim 5 \times 10^{-7}$ K^{-1} [16]) which may allow for higher flexibility in adjusting the coherence length of the fiber.

1.3. Layout of the Paper

This paper is organized as follows: Section 2 details the numerical methods used, while Section 3 provides a description of the ES-PCF structure considered. Section 4 presents detailed results and is divided into subsections: Section 4.1 discusses the effective indices and overlap integral of the fundamental and second harmonic modes, Section 4.2 contains results and discussion on the coherence length and quasi-phase matching (QPM), Section 4.3 discusses the error tolerance in the coherence length, Section 4.4 discusses the power comparison between ES-PCF and PCF for fundamental and second harmonic frequencies, and Section 4.5 presents a comparison of bending loss between ES-PCF and conventional PCF. Finally, Section 5 presents the conclusions of the study.

2. Numerical Method

Initially, the finite element method (FEM) was used for modal analysis. The FEM has been used to obtain the optimum ES-PCF structural parameters for SHG, following which the propagation constant (β) and the generated modal fields are used in the finite element beam propagation method (FE-BPM) to analyze the evolution of the fundamental and second harmonic waves [17]–[20].

For modal analysis using the FEM, the cross section of a waveguide is discretized into a number of triangular elements using an irregular mesh. The FEM, which is based on the vector H-field

[1]Note that electron-beam irradiation cannot be applied to pure silica.

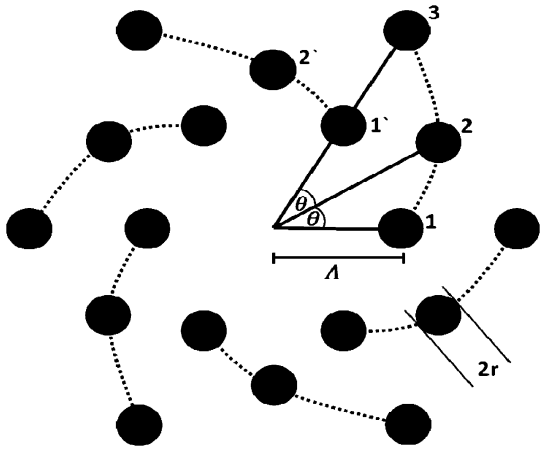

Fig. 1. Structure of the ES-PCF.

formulation, is used to obtain the modal field solutions and propagation constants of the fundamental and higher order quasi-Transverse Electric (TE) and quasi-Transverse Magnetic (TM) modes [21]. The full vector H-field formulation can be written as

$$\omega^2 = \frac{\left(\int (\nabla \times \vec{H}) * \cdot \hat{\varepsilon}^{-1} (\nabla \times \vec{H})\, d\Omega\right) + \left(\int (\eta/\varepsilon_0)(\nabla \cdot \vec{H}) * (\nabla \cdot \vec{H})\, d\Omega\right)}{\int \vec{H} * \cdot \hat{\mu} \vec{H}\, d\Omega} \tag{1}$$

where $\vec{H}$ is the full-vectorial magnetic field; $\hat{\varepsilon}$ and $\hat{\mu}$ are the permittivity and permeability, respectively, of the waveguide; ε_0 is the permittivity of the free space, and ω^2 is the eigenvalue where ω is the angular frequency of the wave. The dimensionless parameter η is used to impose the divergence-free condition of the magnetic field in a least squares sense to eliminate spurious solutions.

3. ES-PCF Design

The structure of the ES-PCF is shown in Fig. 1. The air-hole arrangement of the ES-PCF structure mimics the "spira mirabilis" (equiangular spiral), which is seen in nature in nautilus shells and sunflower heads [5]. This ES pattern of the sunflower head produces the most efficient packing of seeds within the flower head without altering the angle or the shape of the curve, and thus, the air holes in the ES-PCF are arranged in a similar pattern.

In the ES-PCF, each arm of air holes forms a single ES where the angle from the center of the core to adjacent holes of a given arm or ES differs by θ (e.g., the angular increment from hole 1 to hole 2 is θ, and hole 2 to hole 3 is also θ). The diameter (d) of each air hole is fixed at $2r$ where r is the air-hole radius. It should be noted that the equivalent holes of each arm can be considered to form a ring, e.g., the first holes of all the arms form the first ring and the second holes of all the arms form the second ring, and so on. The radius (Λ) of the ES-PCF is defined as the distance between the center of the core and the center of an air hole in the first ring. The radii drawn to the center of air holes on subsequent rings of the same ES, i.e., at intervals of θ, form a geometric progression. The distance between the air holes within a ring increases with the ring number (e.g., the distance between holes 2 and 2′ is larger than the distance between holes 1 and 1′). The main advantage of the ES-PCF is the improved field confinement in comparison to that of conventional PCF. This is due to the hole-orientation of the ES-PCF, where the outer air holes block the field escaping through the material (i.e., interhole region) of the previous ring. The results presented in this paper show that the SH output power of SF57 ES-PCF is considerably higher than that of conventional PCF, e.g., $\sim$2.1 W in ES-PCF as opposed to $\sim$1.6 W in conventional PCF

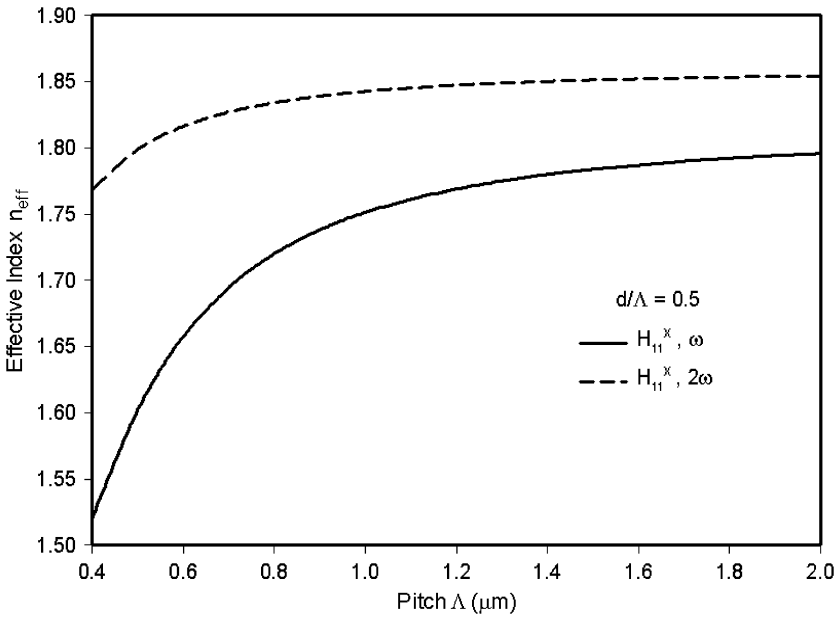

Fig. 2. Variation of the effective indices with the pitch for the first-order mode at ω and 2ω.

after the propagation of 250 μm with a fundamental pump power of 1 kW (continuous wave), operating fundamental wavelength of 1.064 μm, corresponding second harmonic wavelength of 0.532 μm, $d/\Lambda = 0.5$, and $\Lambda = 1.0$ μm, while the ES-PCF design consisted of six arms, four rings, and $\theta = 30^0$.

The ES-PCF structure with air holes arranged in a spiral lattice in the cladding is represented in the simulation by an irregular mesh of 28 800 triangular elements. In this paper, the H_{mn}^x (quasi-TM) and H_{mn}^y (quasi-TE) mode notations are used: The equivalent LP_{mn} notation has been indicated where appropriate.

4. Results

4.1. Modal Properties and SHG in the ES-PCF

The variation of the effective index (n_{eff}) with pitch (Λ) has been studied for the first-order mode at the two frequencies ω and 2ω, and this is shown in Fig. 2. The dispersion properties of SF57 have been considered by using the refractive indices for SF57 and the Sellmeier coefficients of SF57 [15]. Here, $n_{eff} = \beta/k_0$ where β is the propagation constant and k_0 is the wavenumber $(k_0 = 2\pi/\lambda$ where λ denotes the wavelength). The first-order mode H_{11}^x (i.e., HE_{11} or LP_{01}) of the fundamental frequency ω is indicated by H_{11}^x, ω.

As can be seen in Fig. 2, a reduction of the pitch results in a reduction of n_{eff} as the confined mode gets exposed to the first ring of air holes. Initially, the effective indices of the modes reduce slowly, but these decrease rapidly as the modes approach their cutoff conditions. Moreover, the effective index of H_{11}^x, 2ω (i.e., H_{11}^x of the second harmonic frequency) is shown to move toward the cutoff condition at a lower rate than of H_{11}^x, ω. This is because the first-order mode of the higher frequency (i.e., of second harmonic) is more confined in the center than that of the lower frequency. Furthermore, as the pitch is increased, the mode becomes more confined to the core, resulting in n_{eff} asymptotically approaching the refractive index of SF57 (i.e., $n_\omega = 1.81173$ and $n_{2\omega} = 1.85841$).

The overlap integral (Γ) between the interacting fundamental and second harmonic first-order modes (H_{11}^x) directly relates to the efficiency of power transfer between these modes, i.e., a higher

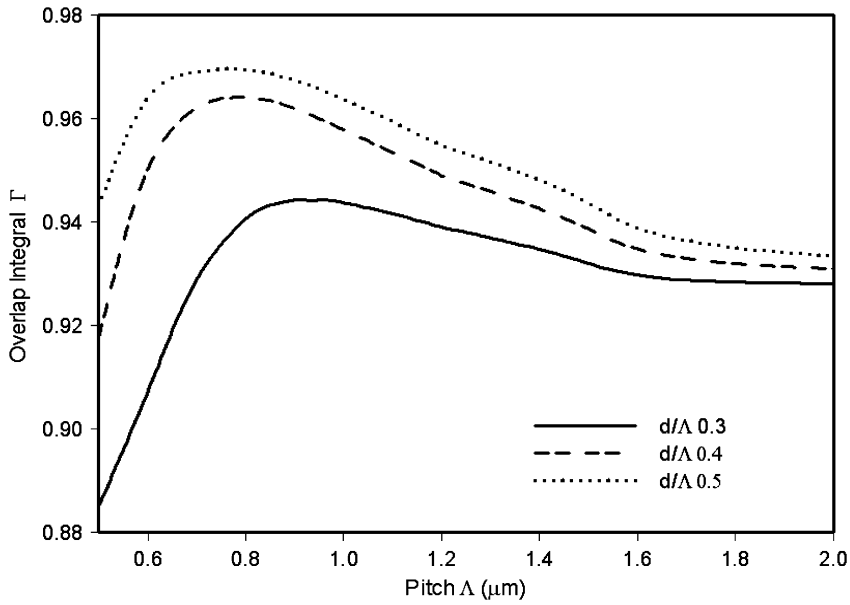

Fig. 3. Variation of the overlap integral with the pitch Λ.

value of the overlap integral results in a higher conversion efficiency and *vice versa* [2]. The definition of the overlap integral is given by

$$\Gamma = \frac{\left|\iint E_{\omega}^{2}.E_{2\omega}.dx.dy\right|}{\left(\iint E_{\omega}^{2}.dx.dy\right).\left(\iint E_{2\omega}^{2}.dx.dy\right)^{1/2}} \tag{2}$$

where E_{ω} and $E_{2\omega}$ are the electric field distribution of the fundamental and second harmonic waves, respectively [22]. Fig. 3 illustrates how the overlap integral of the first-order modes (H_{11}^{x}) for ω and 2ω vary with the pitch (Λ) over a range of d/Λ values.

For a given pitch, the overlap integral increases as d increases. This arises because, as d increases, the equivalent index of the cladding decreases, increasing the index contrast between core and cladding, which in turn increases the confinement of the mode in the ES-PCF. Further, as the pitch decreases for a given value of d/Λ, the overlap integral increases, reaching a maximum value (in the region 0.7 μm $\leq \Lambda \leq$ 1 μm), and then starts to decrease; this can be explained as follows. Reducing the pitch makes H_{11}^{x}, ω and H_{11}^{x}, 2ω more confined which reduces the mismatch of their effective areas leading to an increase in the overlap integral. However, at very small pitch values the fundamental field reaches its cutoff region faster than the second harmonic field. Therefore, even though the second harmonic field becomes more confined to the core, the mismatch between fundamental and second harmonic fields becomes significant and the overlap integral starts to reduce at very small Λ values.

The overlap integral (Γ) and the second harmonic susceptibility tensor values (d_{ij}) are key parameters in determining the rate of power conversion. High SH power can be gained by d_{ij} values which are material properties; indeed, the d_{ij} values of SF57 (i.e., $d_{33} \sim 0.35$ pm/V) are high in comparison with that of silica (i.e., $d_{33} \sim 0.22$ pm/V). On the other hand, the overlap between the interacting modes depends on the fiber design. When the fundamental and second harmonic waves are not phase matched, the second harmonic power increases until the waves are out of phase and SH power starts depleting. Fig. 4 shows the variation of the maximum output power (P_{Lc}) with the pitch (Λ), for different d/Λ values, where P_{Lc} is the power after the propagation of one coherence length (L_c) (which is explained in Section 4.2). This value is obtained by FE-BPM, which takes into account all factors, including phase matching.

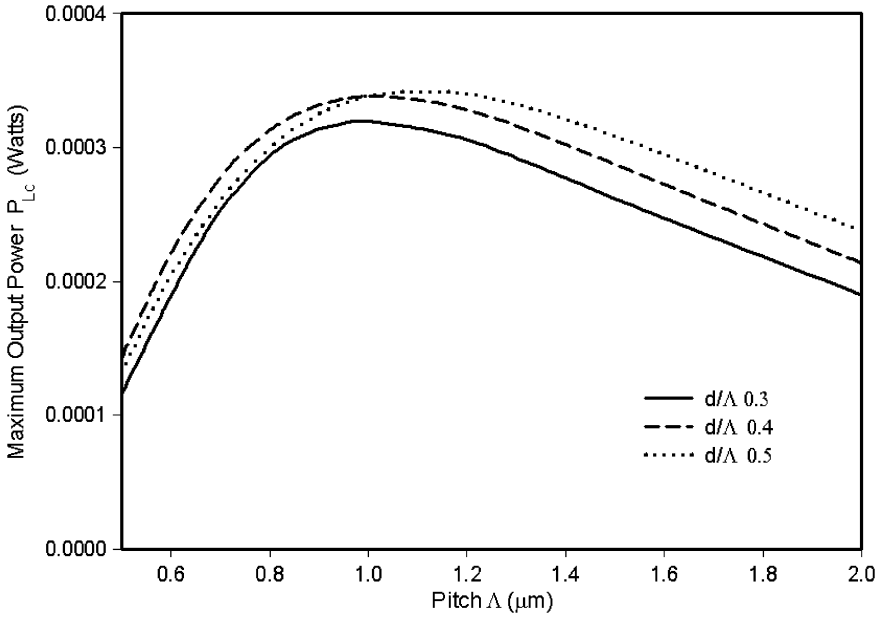

Fig. 4. Variation of the maximum second harmonic output power with the pitch.

It can be observed that a higher d/Λ value yields a higher value of P_{Lc} because as d/Λ increases, the fraction of air increases in the ES-PCF, and the power intensity is more confined in the core. Even though the decreasing of the pitch causes the power to be further confined into the core, once it reaches its threshold, the power spreads into the air region and dissipates, reducing P_{Lc} and hence creating the peak values (in the region 0.9 μm $\leq \Lambda \leq$ 1.1 μm). Further, since the air filling fraction is higher for larger d/Λ values (e.g., $d/\Lambda = 0.5$), the cutoff region is reached faster than in the case of lower d/Λ values (e.g., $d/\Lambda = 0.3$).

4.2. Coherence Length and QPM

The fundamental and second harmonic waves accumulate a phase shift of π over a distance known as the coherence length (L_c). Here, $L_c = \pi/\Delta\beta$ and $\Delta\beta = \beta_{2\omega} - 2\beta_\omega$, where β_ω and $\beta_{2\omega}$ are the propagation constants of the fundamental and second harmonic waves, respectively. The variation of L_c with respect to the pitch is plotted in Fig. 5.

As d/Λ decreases for a given pitch (Λ), the effective index (n_{eff}) increases due to the increased area of the solid SF57 bridges between the air holes: this results in an increase of L_c. Moreover, as the pitch is increased, the SF57 area is further increased and L_c asymptotically approaches the value for bulk SF57 $(\sim 5.69\ \mu\text{m})$. As the effective index increases, the propagation constant (β) also increases. As seen in Fig. 2, for higher Λ values, β_ω increases faster than $\beta_{2\omega}$, bringing $2\beta_\omega$ close to $\beta_{2\omega}$ (i.e., $2\beta_\omega \approx \beta_{2\omega}$), which results in a higher value of L_c. Further, the ideal condition occurs when $n^\omega = n^{2\omega}$ (where n^ω and $n^{2\omega}$ are the fundamental and second harmonic refractive indices, respectively), which cannot be realized in practice due to the chromatic dispersion of the material.

The direction of power flow between the fundamental and second harmonic waves depends on their relative phase of the fundamental and second harmonic waves and hence this changes sign for a distance equal to every coherence length. To overcome this problem, the QPM technique can be applied, i.e., by changing the sign of the nonlinear susceptibility (χ^2) at every L_c, the phase of the polarization wave is shifted by π, effectively rephasing the interaction and leading to monotonic power flow into the second harmonic wave [23]. Changing the sign of χ^2 can be achieved by using poling techniques.

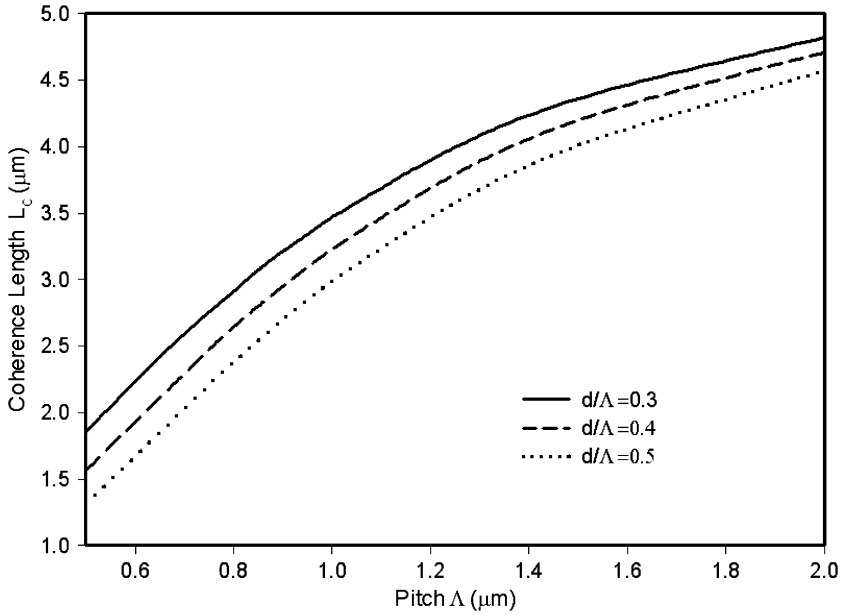

Fig. 5. Variation of the coherence length (L_c) with the pitch (Λ).

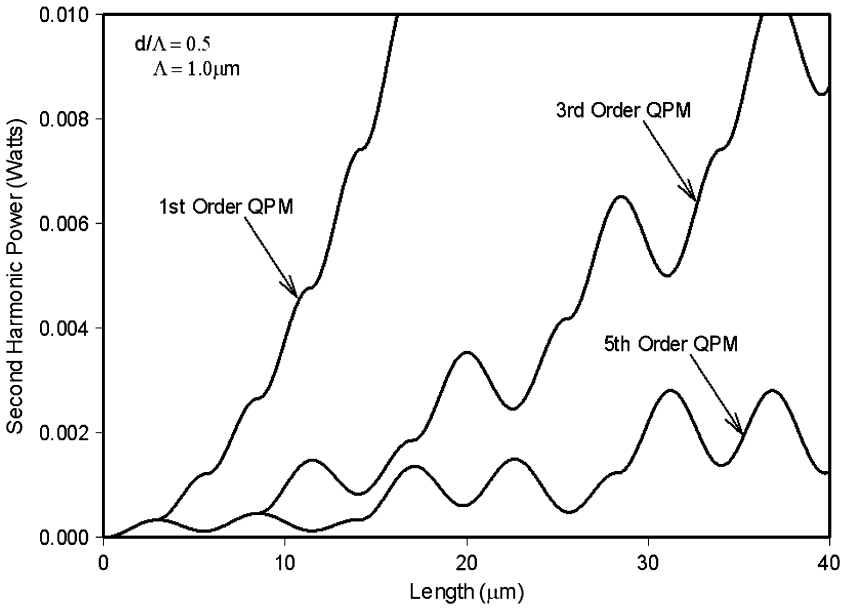

Fig. 6. Generated second harmonic power with first-, third-, and fifth-order QPM.

The most rapid growth of the second harmonic output power can be achieved by changing the sign of χ^2 for every L_c (which is known as first-order QPM), as shown in Fig. 6 (for $d/\Lambda = 0.5$ and $\Lambda = 1.0$ μm).

Changing the sign of χ^2 at every value of L_c (i.e., $\sim$2.9 μm) along the fiber length is challenging in practice. Hence, higher order QPM can be considered instead, i.e., nth-order phase matching can be achieved by poling with a period of nL_c. The QPM for the first-, third-, and fifth-order modulations are shown in Fig. 6. Note that higher order QPMs need a longer propagation distance to reach a given level of SH output power within the fiber when compared with lower order ones.

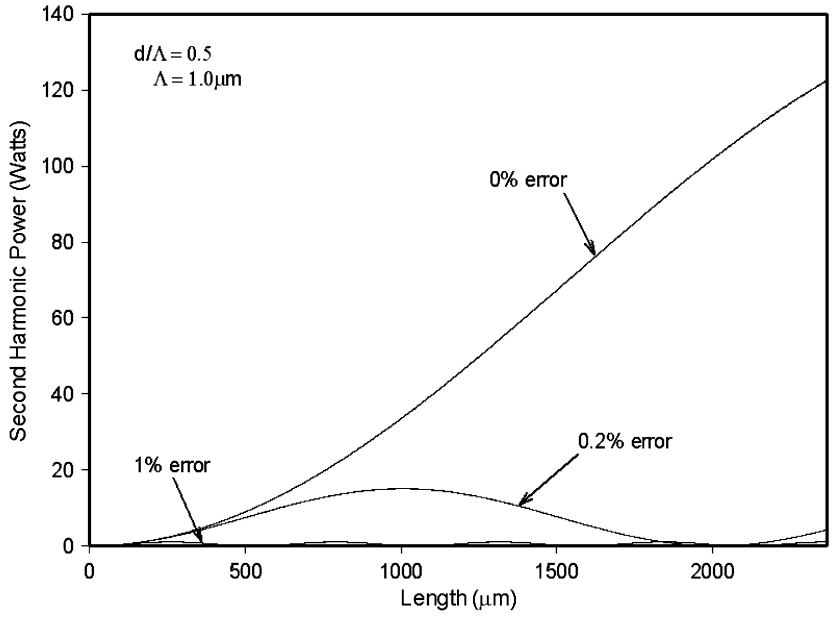

Fig. 7. Effect of fabrication tolerance on second harmonic output power with first-order QPM.

However, this difference in the micrometer range causes no problems, given the length of a fiber in practice, and in fact, higher order QPMs make the fabrication process easier, especially in the case of short coherence lengths.

4.3. Error Tolerance in QPM

During the fabrication process, an error denoted by ΔL_c can occur, which is defined as the difference between the desired coherence length and the actual coherence length achieved after the fabrication. Assuming that the fundamental frequency propagates through N periodically poled regions, and the second harmonic output power builds up along the length of the ES-PCF, the accumulated error in length after propagating a distance NL_c is given by $N\Delta L_c$. After a distance of propagation during which the accumulated length error becomes equal to the coherence length, the phase mismatch is equal to π, and the power starts to reduce [18]. This behavior can be observed in Figs. 7 and 8 for first-order and fifth-order QPM, respectively.

It can be seen that with the first-order QPM, the maximum SH output power for the 0% error case (i.e., no fabrication error) reaches a value of $\sim$120 W (and $\sim$5.6 W with fifth-order QPM) over a distance of $\sim$2350 μm, while a 0.2% error reduces the maximum power to $\sim$15 W (and $\sim$0.7 W with fifth-order QPM) for the same distance. Therefore, once a reasonable coherence length is achieved by using poling techniques, it is important to fine-tune by employing techniques such as temperature tuning period of the Bragg grating [24] or strain period of a long period grating [25] to minimize the error.

4.4. Second Harmonic Power Comparison

Fig. 9 shows the first-order quasi-phase matched SH output power for ES-PCF (SF57) and PCF (silica and SF57) with varied numbers of air holes. In all the cases, $d/\Lambda = 0.5$, and $\Lambda = 1.0$ μm.

It is clear that as the number of air holes is increased, the SH power improves for both conventional PCF and ES-PCF. The SH power can be further improved by employing the ES-PCF structure (instead of conventional PCF) and the SF57 material (instead of silica). Considering curves a) and c), i.e., conventional PCF with silica and SF57, respectively, both with 40 air holes, it can be seen clearly that the SH output power of curve c) is much higher, which is due to the high d_{33} value of the SF57 material. The superiority of the ES-PCF structure is clearly illustrated by curve d),

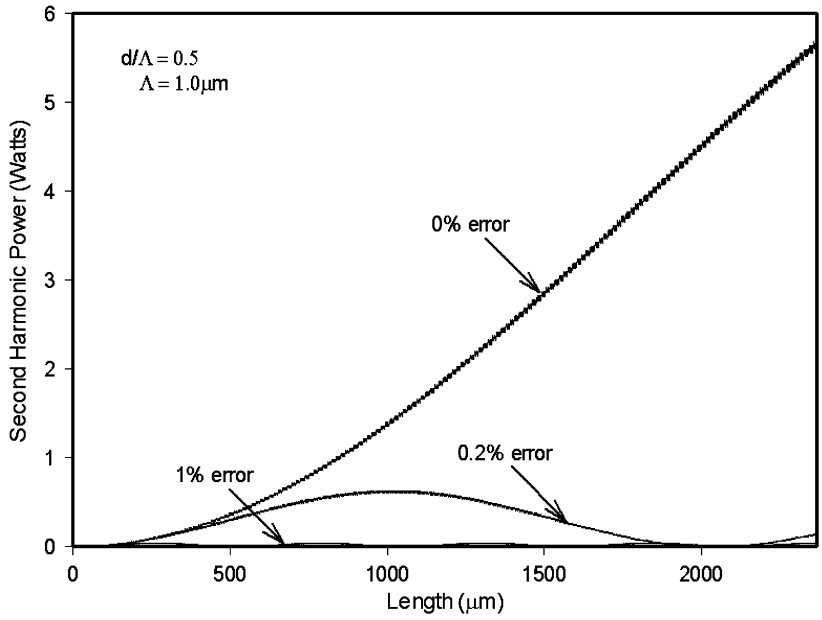

Fig. 8. Effect of fabrication tolerance on second harmonic output power with fifth-order QPM.

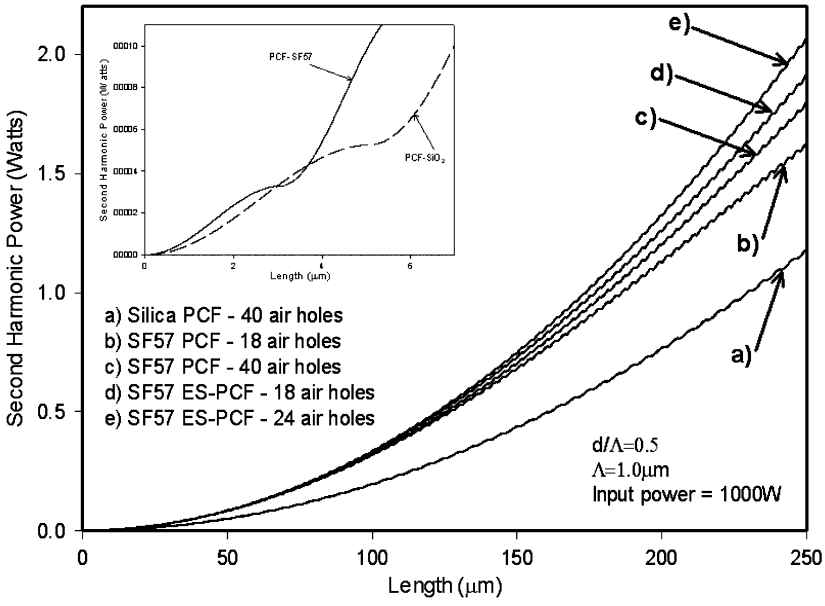

Fig. 9. Comparison of quasi-phase matched second harmonic output power with length for different PCF structures and different materials. The inset graph shows an enlarged version of curves a) and c) for the propagation of a single coherence length.

i.e., ES-PCF with 18 air holes, which has a considerably higher output power (∼19 W) than that of curve b) (∼1.6 W), i.e., PCF with the same number of air holes (and same material); and still higher compared with that of curve c) (∼1.8 W), i.e., PCF with almost twice the number of air holes (i.e., 40). Moreover, curve e) shows that the SH output power (∼2.1 W) can be further improved by increasing the number of air holes (i.e., 24 air holes) in the ES-PCF. This improvement is already seen at a propagation length of 250 μm and will be much more significant with further propagation.

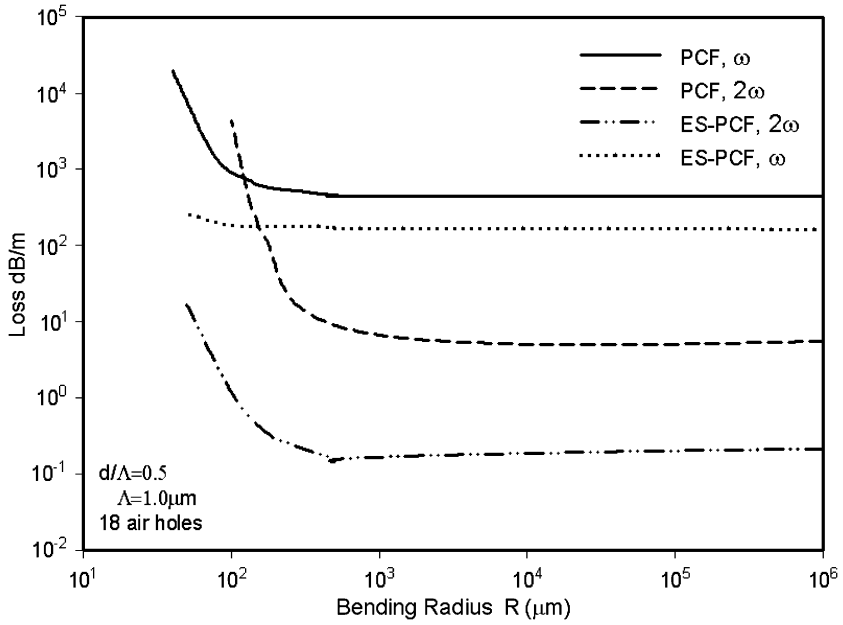

Fig. 10. Comparison of the bending loss as a function of the bending radius for ES-PCF and PCF with fundamental and second harmonic frequencies.

The difference between the two structures is a result of the superior confinement of the mode in the core region in ES-PCF, which results in a better overlap integral compared with that of the conventional PCF structure.

The inset graph shows an enlarged version of curves a) and c) for the propagation over a single coherence length. The value of L_c of silica is higher than that of SF57 which is due to the lower material refractive index difference between the fundamental and the SH waves (i.e., for SF57 $\Delta n = 0.0467$, for SiO_2 $\Delta n = 0.0097$). The inset graph shows clearly that the SH output power is higher in silica after the propagation of a distance equal to one L_c. Nevertheless, as mentioned above, observations made at further propagation lengths show that SF57 leads to a higher level of power compared with silica while the ES-PCF structure helps further increase the power.

4.5. Bending Loss

Bending and leakage losses are important factors to consider when determining performance and practical implementation of the PCF/ES-PCFs. The modal properties of the bending loss have been analyzed by full vectorial complex FEM with perfectly matching layer (PML). Both types of structures suffer from bending loss due to the bend curvature creating an angle that is too sharp for the field to be reflected back into the core, causing some of the field to radiate from the fiber cladding. Further, it is well known that an optical fiber suffers from increased bending loss as it reaches its critical bending radius. However, bending can also be exploited to fine-tune the modal properties of a PCF, and in this case the phase matching of the fundamental and second harmonic waves. The effect of bending can be modeled by converting a bent fiber to its equivalent straight fiber with a modified refractive index profile. The coordinate transformation allows a bent optical waveguide in the x plane to be represented by an equivalent straight waveguide with a modified refractive index distribution $n_{eq}(x, y)$, and thus

$$n_{eq}(x, y) = n(x, y)\left(1 + \frac{x}{R}\right) \tag{3}$$

where $n(x, y)$ is the original refractive index profile of the bent waveguide, $n_{eq}(x, y)$ is the equivalent refractive index profile of a straight guide, R is the radius of the curvature, and x is the

distance from the center of the waveguide [26]. It was observed that coherence length can be adjusted up to 3% by introducing a bending in these PCFs (results are not shown here). However, bending a PCF also introduces a resulting bending loss. Bending and leakage losses can be reduced by increasing the number of air holes, although this generally adds to the fabrication costs. Previously, it has been shown that ES-PCF suffers from lower leakage and bending losses, as the second ring of air holes can be placed more effectively [27]. Fig. 10 shows the comparison of the bending loss as a function of the bending radius in ES-PCF and PCF designs in SF57 for both the fundamental and second harmonic waves.

In this case, the number of air holes is taken to be 18 for both ES-PCF and PCF. As seen in Fig. 10, the bending loss in ES-PCF is significantly lower than that of PCF for the fundamental frequency. A similar behavior can be observed in ES-PCF and PCF for the SH frequency but with lower loss as the modes are well confined. The low confinement loss occurs due to the unique orientation of the air holes of the ES-PCF structure [28]. When the bending radius is decreased, the air holes in the outer rings in ES-PCF (which are positioned between the air holes of the inner rings) prevent the mode escaping through the SF57 bridges. However, both bending and leakage losses can be further reduced by increasing the number of air holes. For a given number of air holes, ES-PCF suffers lower bending and leakage loss than the conventional PCF, particularly when the number of air holes is modest, which reduces fabrication costs while also making such ES-PCF easy to handle for practical applications.

5. Conclusion

In this paper, numerically simulated results show that a significantly higher level of SH output power can be achieved by employing the ES-PCF design in SF57 soft glass rather than conventional silica PCF. For example, a power increase of 31% was numerically demonstrated from conventional PCF ($\sim$1.6 W) to ES-PCF ($\sim$2.1 W) for a propagation length of 250 μm. The higher output power is a result of the higher overlap integral due to the better modal properties in ES-PCF. The QPM technique has been applied to achieve maximum SH output power. It has been shown that potential fabrication tolerances lead to errors in the coherence length, which could result in a substantial reduction in the generated quasi-phase matched SH power. However, it is possible to minimize fabrication errors by temperature or strain tuning. Moreover, the ability of the ES-PCF structure to effectively control the modal field gives rise to ultralow bending loss which would be easy to handle; this is a significant advantage over conventional PCF, and furthermore, bending can also be exploited in the adjustment of phase matching.

References

[1] D. Fluck, T. Pliska, P. Günter, S. Bauer, L. Beckers, and C. Buchal, "Blue-light second-harmonic generation in ion-implanted $KNbO_3$ channel waveguides of new design," *Appl. Phys. Lett.*, vol. 69, no. 27, pp. 4133–4135, Dec. 1996.
[2] G. P. Agrawal, "Nonlinear fiber optics," in *Quantum Electronics—Principles and Applications,* 4th ed. Amsterdam, The Netherlands: Elsevier, 2007, p. xvi-559.
[3] T. M. Monro, V. Pruneri, N. G. R. Broderick, D. Faccio, P. G. Kazansky, and D. J. Richardson, "Broad-band second-harmonic generation in holey optical fibers," *IEEE Photon. Technol. Lett.*, vol. 13, no. 9, pp. 981–983, Sep. 2001.
[4] J. C. Knight, T. A. Birks, P. S. Russell, and D. M. Atkin, "All-silica single-mode optical fiber with photonic crystal cladding," *Opt. Lett.*, vol. 21, no. 19, pp. 1547–1549, Oct. 1996.
[5] A. Agrawal, N. Kejalakshmy, B. M. A. Rahman, and K. T. V. Grattan, "Soft glass equiangular spiral photonic crystal fiber for supercontinuum generation," *IEEE Photon. Technol. Lett.*, vol. 21, no. 22, pp. 1722–1724, Nov. 2009.
[6] R. A. Myers, N. Mukherjee, and S. R. J. Brueck, "Large 2nd-order nonlinearity in poled fused-silica," *Opt. Lett.*, vol. 16, no. 22, pp. 1732–1734, Nov. 1991.
[7] D. Faccio, A. Busacca, W. Belardi, V. Pruneri, P. G. Kazansky, T. M. Monro, D. J. Richardson, B. Grappe, M. Cooper, and C. N. Pannell, "Demonstration of thermal poling in holey fibers," *Electron. Lett.*, vol. 37, no. 2, pp. 107–108, Jan. 2001.
[8] V. Pruneri, G. Bonfrate, P. G. Kazansky, C. Simonneau, P. Vidakovic, and J. A. Levenson, "Efficient frequency doubling of 1.5 μm femtosecond laser pulses in quasi-phase-matched optical fibers," *Appl. Phys. Lett.*, vol. 72, no. 9, pp. 1007–1009, Mar. 1998.
[9] V. Pruneri and P. G. Kazansky, "Electric-field thermally poled optical fibers for quasi-phase-matched second-harmonic generation," *IEEE Photon. Technol. Lett.*, vol. 9, no. 2, pp. 185–187, Feb. 1997.
[10] H. Takebe, P. G. Kazansky, P. S. J. Russell, and K. Morinaga, "Effect of poling conditions on second-harmonic generation in fused silica," *Opt. Lett.*, vol. 21, no. 7, pp. 468–470, Apr. 1996.

[11] P. G. Kazansky, A. Kamal, and P. S. J. Russell, "High second-order nonlinearities induced in lead silicate glass by electron-beam irradiation," *Opt. Lett.*, vol. 18, no. 9, pp. 693–695, May 1993.
[12] M. X. Qiu, F. Pi, and G. Orriols, "The role of lead component in second-harmonic generation in lead silica by electron-beam irradiation," *Appl. Phys. Lett.*, vol. 73, no. 21, pp. 3040–3042, Nov. 1998.
[13] M. Feng, A. K. Mairaj, D. W. Hewak, and T. M. Monro, "Nonsilica glasses for holey fibers," *J. Lightw. Technol.*, vol. 23, no. 6, pp. 2046–2054, Jun. 2005.
[14] N. A. Wolchover, F. Luan, A. K. George, J. C. Knight, and F. G. Omenetto, "High nonlinearity glass photonic crystal nanowires," *Opt. Exp.*, vol. 15, no. 3, pp. 829–833, Feb. 2007.
[15] *Optical Glass (Schott Glass)*, 2010, retrieved Dec. 7, 2010. [Online]. Available: http://www.us.schott.com/advanced_optics/us/abbe_datasheets/schott_datasheet_sf57.pdf
[16] D. Wong, "Thermal-stability of intrinsic stress birefringence in optical fibers," *J. Lightw. Technol.*, vol. 8, no. 11, pp. 1757–1761, Nov. 1990.
[17] F. A. Katsriku, B. M. A. Rahman, and K. T. V. Grattan, "Numerical modeling of second harmonic generation in optical waveguides using the finite element method," *IEEE J. Quantum Electron.*, vol. 33, no. 10, pp. 1727–1733, Oct. 1997.
[18] F. A. Katsriku, B. M. A. Rahman, and K. T. V. Grattan, "Finite-element analysis of second-harmonic generation in AlGaAs waveguides," *IEEE J. Quantum Electron.*, vol. 36, no. 3, pp. 282–289, Mar. 2000.
[19] P. S. Weitzman and U. Osterberg, "A modified beam-propagation method to model second-harmonic generation in optical fibers," *IEEE J. Quantum Electron.*, vol. 29, no. 5, pp. 1437–1443, May 1993.
[20] H. M. Masoudi and J. M. Arnold, "Modeling second-order nonlinear effects in optical wave-guides using a parallel-processing beam-propagation method," *IEEE J. Quantum Electron.*, vol. 31, no. 12, pp. 2107–2113, Dec. 1995.
[21] B. M. A. Rahman and J. B. Davies, "Finite-element solution of integrated optical waveguides," *J. Lightw. Technol.*, vol. 2, no. 5, pp. 682–688, Oct. 1984.
[22] C. Flueraru and C. P. Grover, "Overlap integral analysis for second-harmonic generation within inverted waveguide using mode dispersion phase match," *IEEE Photon. Technol. Lett.*, vol. 15, no. 5, pp. 697–699, May 2003.
[23] D. S. Hum and M. M. Fejer, "Quasi-phase matching," *Comptes Rendus Phys.*, vol. 8, pp. 180–198, 2007.
[24] C. Martelli, J. Canning, N. Groothoff, and K. Lyytikainen, "Strain and temperature characterization of photonic crystal fiber Bragg gratings," *Opt. Lett.*, vol. 30, no. 14, pp. 1785–1787, Jul. 2005.
[25] V. Bhatia and A. M. Vengsarkar, "Optical fiber long-period grating sensors," *Opt. Lett.*, vol. 21, no. 9, pp. 692–694, May 1996.
[26] M. Heiblum and J. H. Harris, "Analysis of curved optical-waveguides by conformal transformation," *IEEE J. Quantum Electron.*, vol. QE-11, no. 2, pp. 75–83, Feb. 1975.
[27] B. M. A. Rahman, N. Kejalakshmy, M. Uthman, A. Agrawal, T. Wongcharoen, and K. T. V. Grattan, "Mode degeneration in bent photonic crystal fiber study by using the finite element method," *Appl. Opt.*, vol. 48, no. 31, pp. 131–138, Nov. 2009.
[28] A. Agrawal, N. Kejalakshmy, M. Uthman, B. M. A. Rahman, and K. T. V. Grattan, "Ultra low bending loss spiral photonic crystal fibers in Terahertz regime," in *Proc. CLEO*, May 1–6, 2011, pp. 1–2.